Acta Pharmaceutica Sinica B 2025;15(6):3041−3058

Chinese Pharmaceutical Association
Institute of Materia Medica, Chinese Academy of Medical Sciences

Acta Pharmaceutica Sinica B

www.elsevier.com/locate/apsb
www.sciencedirect.com

ORIGINAL ARTICLE

SRSF7 promotes pulmonary fibrosis through regulating PKM alternative splicing in lung fibroblasts

Tongzhu Jin[a,b,†], Huiying Gao[a,†], Yuquan Wang[a,c,†], Zhiwei Ning[a,†], Danyang Bing[a], Yan Wang[a], Yi Chen[a], Xiaomu Tian[a], Qiudi Liu[a], Zhihui Niu[a], Jiayu Guo[a], Jian Sun[d], Ruoxuan Yang[a], Qianqian Wang[a], Shifen Li[a], Tianyu Li[a], Yuhong Zhou[e], Wenxin He[f,*], Yanjie Lu[a,*], Yunyan Gu[a,c,*], Haihai Liang[a,b,g,*]

[a]*State Key Laboratory of Frigid Zone Cardiovascular Diseases (SKLFZCD), Department of Pharmacology (State Key Labratoray-Province Key Laboratories of Biomedicine-Pharmaceutics of China, Key Laboratory of Cardiovascular Research, Ministry of Education), College of Pharmacy, Harbin Medical University, Harbin 150081, China*
[b]*Department of Nephrology, the Second Affiliated Hospital of Harbin Medical University, Harbin 150081, China*
[c]*Department of Systems Biology, College of Bioinformatics Science and Technology, Harbin Medical University, Harbin 150081, China*
[d]*Translational Medicine Research Center, Medical Pathology Center, Chongqing University Three Gorges Hospital, School of Medicine Chongqing University, Chongqing University, Chongqing 400000, China*
[e]*Department of Basic Medicine, Xiamen Medical College, Xiamen 361023, China*
[f]*Department of Thoracic Surgery, Shanghai Pulmonary Hospital, Tongji University, Shanghai 200433, China*
[g]*Research Unit of Noninfectious Chronic Diseases in Frigid Zone (2019RU070), Chinese Academy of Medical Sciences, Harbin 150081, China*

Received 5 December 2024; received in revised form 7 February 2025; accepted 3 March 2025

KEY WORDS

IPF;
Alternative splicing;

Abstract Idiopathic pulmonary fibrosis (IPF), a chronic interstitial lung disease, is characterized by aberrant wound healing, excessive scarring and the formation of myofibroblastic foci. Although the role of alternative splicing (AS) in the pathogenesis of organ fibrosis has garnered increasing attention, its

*Corresponding authors.
E-mail addresses: lianghaihai@ems.hrbmu.edu.cn (Haihai Liang), guyunyan@ems.hrbmu.edu.cn (Yunyan Gu), yjlu2008@163.com (Yanjie Lu), awen_he@126.com (Wenxin He).
[†]These authors made equal contributions to this work.
Peer review under the responsibility of Chinese Pharmaceutical Association and Institute of Materia Medica, Chinese Academy of Medical Sciences.

https://doi.org/10.1016/j.apsb.2025.04.017

Splicing factor;
SRSF7;
PKM;
Fibroblasts;
Metabolism;
Drug screening

specific contribution to pulmonary fibrosis remains incompletely understood. In this study, we identified an up-regulation of serine/arginine-rich splicing factor 7 (SRSF7) in lung fibroblasts derived from IPF patients and a bleomycin (BLM)-induced mouse model, and further characterized its functional role in both human fetal lung fibroblasts and mice. We demonstrated that enhanced expression of Srsf7 in mice spontaneously induced alveolar collagen accumulation. Mechanistically, we investigated alternative splicing events and revealed that SRSF7 modulates the alternative splicing of pyruvate kinase (PKM), leading to metabolic dysregulation and fibroblast activation. *In vivo* studies showed that fibroblast-specific knockout of *Srsf7* in conditional knockout mice conferred resistance to bleomycin-induced pulmonary fibrosis. Importantly, through drug screening, we identified lomitapide as a novel modulator of SRSF7, which effectively mitigated experimental pulmonary fibrosis. Collectively, our findings elucidate a molecular pathway by which SRSF7 drives fibroblast metabolic dysregulation and propose a potential therapeutic strategy for pulmonary fibrosis.

1. Introduction

Idiopathic pulmonary fibrosis (IPF), the quintessential form of fibrotic lung disease, is characterized by uncontrolled fibroblast proliferation and excessive deposition of extracellular matrix (ECM), ultimately leading to respiratory failure and death. This pathological process can be triggered by various factors, including toxin exposure, infections, and severe trauma[1,2]. Although pirfenidone and nintedanib have been approved for IPF treatment, these therapies only slow disease progression rather than halt or reverse it[3]. Therefore, a deeper understanding of the underlying mechanisms driving IPF is essential for developing more effective therapeutic interventions.

Myofibroblasts, which originate from the differentiation of lung fibroblasts, have been identified as the key effector cells in the progression of IPF. Myofibroblasts and fibroblasts play a critical role in the excessive deposition of ECM and the subsequent structural deterioration of lung tissue[4,5]. Research has demonstrated that the accumulation of fibroblasts in IPF is driven by their activation and subsequent invasion into the underlying ECM. Notably, fibroblasts derived from the lung tissues of IPF patients or animal models exhibit an enhanced capacity for ECM invasion[6,7]. Recent studies have highlighted that therapeutic strategies targeting fibroblast activation can significantly improve lung function in IPF patients. Several biological processes, including oxidative stress, alternative splicing, and metabolic reprogramming, have been implicated in fibroblast activation[8-10].

Alternative splicing is an intricate and evolutionarily conserved post-transcriptional mechanism that generates numerous mRNA variants and contributes to the significant protein diversity observed in eukaryotic organisms[11,12]. Given that the vast majority of human genes contain introns, and approximately 93% of these genes undergo alternative splicing, it is not surprising that disruptions in normal mRNA splicing patterns can result in a variety of human diseases[13-15]. High-throughput sequencing studies have demonstrated that alternative splicing plays a pivotal role in a range of disease processes, including cancer, cardiovascular diseases, and numerous genetic disorders, with particularly notable implications in fibrotic diseases[16]. In the context of pulmonary fibrosis, Nicholas et al. discovered that an alternative splicing isoform of vascular endothelial growth factor (VEGF-A165b) was upregulated in lung tissue, isolated lung fibroblasts, and plasma from patients with IPF[17]. Furthermore, it has been suggested that the formation of the EDA^+ fibronectin 1 (Fn1) splicing isoform can exacerbate inflammatory, fibronectin-related diseases by activating toll-like receptors[18]. To modulate alternative splicing events, various strategies have been developed, including the regulation of auxiliary *cis*-elements and the recruitment of the spliceosome, a complex composed of splicing factors and small nuclear ribonucleoproteins (snRNPs) such as U1, U2, U4, U5, and U6[19,20]. Splicing factors, such as serine/arginine-rich splicing factors (SRSFs) and heterogeneous nuclear ribonucleoproteins (hnRNPs), are engaged by pre-mRNA in a sequence-specific manner[11]. However, the precise mechanisms by which alternative splicing sustains a profibrotic phenotype and contributes to the progression of IPF remain to be elucidated. Serine/arginine-rich proteins constitute a crucial family of splicing factors that govern RNA splicing and other RNA modification-related events, comprising 12 members[21]. Modulating the expression and localization of SR proteins can significantly impact RNA binding, splicing site recognition, transcriptional elongation, and the cellular response to DNA damage[11]. Notably, only SRSF1, SRSF7, and SRSF10 have been identified as proteins capable of shuttling between the nucleus and the cytoplasm[22]. The majority of SR proteins function as splicing activators, facilitating exon recognition and enabling selective regulation of exon inclusion or exclusion[11]. For instance, Chen et al.[23] demonstrated that SRSF5 induces abnormal exon skipping of METTL14 and Cyclin L2, thereby promoting the growth and metastasis of pancreatic cancer cells.

Splicing factor SRSF2 has been reported as a key regulator of cell survival and implicated in myoblast proliferation and myogenesis by regulating the alternative splicing events of MYH5[24]. SRSF7 has been shown to mediate age-dependent alternative splicing events and to participate in apoptosis in colon and lung cancer cells[25]. Beyond their role in determining transcript length and sequence composition, SR proteins also exert control over gene expression at various stages of RNA metabolism, including mRNA output, stability, and translation[26,27]. In our previous study, we demonstrated that SRSF1 regulates the alternative splicing event of *FN1*, which plays an important role in idiopathic pulmonary fibrosis[28]. However, the specific roles of the RNA spliceosome and splicing factors in pulmonary fibrosis remain to be more deeply explored.

In this study, increased expression of SRSF7 was detected in the lung tissue of IPF patients and bleomycin-treated mice, suggesting that SRSF7 may play an essential role in pulmonary

fibrosis. Consistent with these findings, we further explored its function and mechanisms in IPF. Moreover, we aimed to screen drugs targeting SRSF7 from the FDA-approved compound library, thus providing a novel strategy for the prevention and treatment of lung fibrosis.

2. Materials and methods

2.1. Human samples

IPF lung tissues were obtained from patients undergoing a lung transplant surgery, and the lung control samples were peri-carcinomatous derived from lung cancer patients at the Shanghai Pulmonary Hospital (Shanghai, China). All donors have given informed consent for the purpose of lung tissues. All studies associated with human tissues were performed in compliance with the Ethic Committee of Shanghai Pulmonary Hospital (K24-015, China).

2.2. Animal models

Srsf7$^{fl/fl}$ and *Col1a2*-CreERT2 were purchased from Cyagen (Cyagen Biosciences) and wild-type C57BL/6 mice (22−25 g) were purchased from Liaoning Changsheng Biotechnology (Benxi, China). *Srsf7*$^{fl/fl}$ and *Col1a2*-CreERT2 mice were cross-bred to generate *Srsf7*$^{fl/fl}$;*Col1a2*-CreERT2 transgenic mice, hereafter referred to as *Srsf7*-cKO mice.

Mice aged 6−8 weeks, with an average body weight of 20−22 g, were intratracheally injected with bleomycin (BLM, 3 mg/kg, Selleck, Shanghai, China) or saline after being anesthetized. After 21 days, the pulmonary fibrosis model was considered to be established. Upon euthanasia, the lungs were collected and snap-frozen for subsequent experiments.

To determine the role of lomitapide *in vivo*, mice were intratracheally injected with bleomycin or saline. After one week, the BLM-treated mice were randomly assigned to two treatment groups. Lomitapide (10 mg/kg, Selleck, Shanghai, China) and Pirfenidone (300 mg/kg, Selleck, Shanghai, China) as positive control are intragastric administration into BLM-treated mice. After two weeks, the mice were euthanized, and lung tissues were collected for subsequent experiments.

All animal experiments were approved by the Harbin Medical University Animal Ethical committee (No. IRB5034621) and conformed to the Declaration of Helsinki. Animals were randomly assigned for each experimental group. Assessors were un-blinded to group allocation.

2.3. Micro-CT

Mice were scanned using a PerkinElmer Quantum GXII microCT scanner. For the scan conditions, the parameters for microCT were 60 kVp for the X-ray tube voltage, and the images were acquired at a resolution of 50 μm. The images were reconstructed using Hiscan Reconstruct software and analysed using Hiscan Analyzer software.

2.4. Pulmonary function test

The mice were anesthetized using sodium pentobarbital and subsequently intubated. Lung function was measured using the Buxco DSI system (Buxco DSI, St. Paul, USA) and evaluated based on parameters such as forced vital capacity (FVC), inspiratory capacity (IC), and lung compliance.

2.5. Cell culture and treatment

The human fetal lung fibroblast (MRC-5) cell line and the human adult lung fibroblast (HLFs) cell line were obtained from Pricella Biotechnology (Wuhan, China). MRC-5 cells were cultured in MEM culture medium supplemented with 10% fetal bovine serum (FBS) and 1% penicillin−streptomycin solution. HLFs were cultured in a specialized medium containing growth factors and 10% FBS. Both cell types were maintained at 37 °C in a cell incubator with a humidified atmosphere of 5% CO_2. profiling, and the cells were tested to be free of mycoplasma contamination.

Cells were transfected when the confluence of MRC-5 cells and HLFs in the cell plate reached 70%−80%. The final concentration of plasmid (*SRSF7/PKM/PKMΔE2*) and siRNA (si-*SRSF7*) (Genecreate, Wuhan, China) was 1 ng/μL and 5 nmo/L, respectively. First, the complete cell medium was replaced with serum-free DMEM. Authentication of the MRC-5 cell line was confirmed by short tandem repeat (STR) M culture medium, and the prepared lipo2000 with plasmid was added into the cell. After 6 h, the culture medium was replaced with normal complete culture medium. The cells were cultured in the medium containing TGF-β1 (10 ng/mL, Sigma−Aldrich, USA) for 24 h before being collected for further analysis. siRNA sequences are displayed in Supporting Information Table S1.

2.6. Western blot

Proteins were extracted from tissues and cells, and then electrophoretic experiments are performed in 10% SDS-PAGE gel. Next, the proteins were transferred to the nitrocellulose membrane, blocked with 5% skim milk. The antibody against FN1 (1:500, Proteintech, Wuhan, China), SRSF7 (1:500, Proteintech, Wuhan, China), α-SMA (1:500, Affinity Biosciences, OH, USA), and β-actin (1:500, Proteintech, Wuhan, China) was incubated at 4 °C overnight. The protein bands were developed and analyzed by Odyssey infrared imaging system.

2.7. Quantitative real-time PCR (qRT-PCR)

Total RNA was extracted using TRIzol reagent (Invitrogen, Carlsbad, USA). The concentration and purity of the RNA were assessed using a NanoDrop 8000 spectrophotometer (Thermo, USA). The RNA was reverse-transcribed into cDNA using a reverse transcription kit (TransGen Biotech, Beijing, China). Quantitative real-time PCR (qRT-PCR) was performed on an ABI 7500 FAST real-time PCR system. The reaction conditions were as follows: 95 °C for 5 min, followed by 40 cycles of 95 °C for 10 s, 55 °C for 15 s, and 72 °C for 20 s. The relative gene expression levels were calculated using the $2^{-\Delta\Delta CT}$ method. PCR products of PKM were analyzed by agarose gel electrophoresis. The primer sequences are listed in Supporting Information Table S2.

2.8. Isolation of primary lung fibroblasts

Primary lung fibroblasts were isolated from the lungs of AAV-*Srsf7*-injection mice and AAV-*NC*-injection mice. Under aseptic conditions, mouse lung tissues were harvested, minced, and transferred into centrifuge tubes on an ultraclean bench. After digestion with collagenase IV (2 mg/mL; Worthington, OH, USA), the supernatant was aspirated, and the reaction was terminated by adding culture medium (90% DMEM

medium + 10% FBS). The resulting suspension was filtered to obtain purified primary lung fibroblasts, which were then centrifuged, resuspended in the same culture medium, and seeded for further culture. After 6 h, non-adherent cells were removed by gentle washing, leaving only adherent primary fibroblasts.

2.9. RNA-seq and data analysis

Total RNA was extracted from MRC-5 cells using TRIzol reagent (Invitrogen, Carlsbad, CA, USA). The quantity and purity of the RNA were analyzed using the Agilent Bioanalyzer 2100 system with the RNA 6000 Nano LabChip Kit (Agilent, CA, USA). Hi-Seq libraries were prepared, and 150 bp paired-end sequencing was performed on an Illumina HiSeq 4000 platform (LC Bio, China) following the manufacturer's recommended protocol. RNA-Seq reads were processed using the HISAT2 software package (version 2.2.1). Initially, low-quality reads were removed based on the quality scores associated with each read. Subsequently, the remaining reads were aligned to the reference genome. Differential gene expression analysis was performed using DESeq2 (version 1.23.10), and gene abundance tables were generated. For heatmap visualization, FPKM-normalized expression values were further normalized using the R package "pheatmap".

All differentially expressed genes (DEGs) were annotated with Gene Ontology (GO) terms from the Gene Ontology database (http://www.geneontology.org/). Enriched GO terms were identified using a hypergeometric test, and the top 20 significantly enriched pathways were selected for visualization. Genes associated with these pathways were imported into the STRING database (*via* the Cytoscape STRING plugin) with a confidence score cutoff of 0.15. No first- or second-step neighbors were included in the analysis. The resulting network consisted of 76 nodes and 556 edges.

Alternative splicing (AS) events were identified and analyzed using rMATS (version 4.1.1; http://rnaseq-mats.sourceforge.net). Significant AS events were defined as those with a false discovery rate (FDR) < 0.05 in pairwise comparisons.

2.10. Histological and immunohistochemical staining

Lung tissue was excised from mice, fixed in 4% paraformaldehyde for 24 h, dehydrated for 20 h, and embedded in paraffin. Sections were dewaxed in xylene, hydrated through an alcohol gradient, and stained with H&E and Masson's trichrome (Solarbio, Beijing, China). For immunohistochemistry, sections were pretreated with 3% hydrogen peroxide, incubated with goat serum, and then incubated overnight with primary antibodies at 4 °C. The next day, sections were incubated with a secondary antibody (HRP-coupled anti-rabbit IgG) and visualized using DAB staining.

2.11. RNA-binding protein immunoprecipitation (RIP)

The MagnaRIPTM Kit (Millipore, USA) was used to perform RNA immunoprecipitation (RIP) following the manufacturer's instructions. Briefly, RIP assays were conducted with SRSF7 or IgG antibodies. MRC-5 cells were collected, lysed, and incubated with SRSF7 or IgG-coated magnetic beads at room temperature. The beads were resuspended in RIP buffer and incubated with the cell lysate at 4 °C overnight. The next day, the RNA/bead complex was washed, digested with proteinase K, and purified. The RNA was analyzed by agarose gel electrophoresis or qRT-PCR, with IgG immunoprecipitation as a negative control.

2.12. Immunofluorescence staining

The lung tissue was sectioned after embedding in OCT compound (SAKURA, Finetek, Japan). Cells and frozen sections were fixed in 4% paraformaldehyde at room temperature or acetone for 5 min, followed by permeabilization with 0.4% Triton X-100 for 8 min. After blocking with BSA, the tissue sections were incubated with primary antibodies, including α-SMA (1:200, Abcam, USA), SRSF7 (1:200, Proteintech, Wuhan, China), and COL1 (1:200, Affinity Biosciences, OH, USA), overnight at 4 °C. The following day, the tissue sections were incubated with fluorescent secondary antibodies and stained with DAPI for nuclear visualization. Fluorescence microscopy was used to observe the immunostaining results.

2.13. EdU cell proliferation assay

Cell proliferation was assessed using the EdU Cell Proliferation Kit (Ruibo Biotechnology, Guangzhou, China). MRC-5 cells were cultured in 24-well plates under standard conditions (37 °C, 5% CO_2). After transfection for 48 h, EdU staining was performed as per the manufacturer's instructions. The stained cells were randomly selected under an inverted fluorescence microscope for image acquisition. The proportion of proliferating cells was quantified using ImageJ software.

2.14. Wound healing assay

MRC-5 cells were cultured in 6-well plates overnight and transfected with different plasmids for 5 h. A 200 μL pipette tip was used to create a uniform scratch. At 0, 24, and 48 h post-scratching, cells were imaged under a Nikon Ts100 microscope. Migration ability was analyzed by measuring the scratch area reduction using ImageJ, which was used to calculate the wound healing rate.

2.15. Cell glucose consumption assay

The consumption of glucose was assessed using the Glucose Assay Kit (Beyotime, Shanghai, China), which employed the *O*-toluidine colorimetric method for quantification at 630 nm, following the manufacturer's protocol. The glucose consumption rate was calculated as the relative reduction in glucose levels in each experimental group compared to the control group.

2.16. Pyruvate kinase activity assay

Pyruvate kinase activity assay kit (Solarbio, Beijing, China) was used to measure PK activity according to the manufacturer's instructions.

2.17. Lactate assay

Lactate was quantified using the Lactate Assay Kit (Solarbio, Beijing, China). Briefly, lactate was enzymatically reacted with a specific enzyme mixture to generate a detectable product. A lactate standard curve was prepared, and the absorbance values of lactate samples (ng/μL) were measured at 570 nm, following the manufacturer's protocol.

2.18. Seahorse assay

The ECAR and OCR were measured using the Seahorse XF96 analyzer (Seahorse Bioscience) following the manufacturer's

instructions. Two days after transfection with PKM, PKMΔE2, and si-SRSF7, MRC-5 cells were seeded on XF96 microplates. After overnight incubation, glycolysis was assessed by sequentially adding glucose (10 mmol/L), oligomycin (1 μmol/L), and 2-DG (50 mmol/L). For the mitochondrial stress test, oligomycin (1 μmol/L), FCCP (0.5 μmol/L), and rotenone/antimycin A (0.5 μmol/L) were sequentially added.

2.19. Cell contraction assay

Cell contractility was measured using the 24-Well Cell Contraction Assay Kit (Cell Biolabs, Shanghai, China). Cells (2×10^6−5×10^6 cells/mL) were resuspended in cold Collagen Gel Working Solution to form the cell contraction matrix. A volume of 250 μL of the matrix was added to each well of the 24-well plate, followed by incubation for 1 h for collagen polymerization. After polymerization, 500 μL of medium was added to each well and replaced with 250 μL of fresh medium daily. Contractility was recorded at 0, 24, and 48 h.

2.20. Statistics and analysis

Data are presented as the mean ± standard error of the mean (SEM) from independent experiments. Statistical significance was assessed using a two-tailed *t*-test or one-way ANOVA. A *P*-value<0.05 was considered statistically significant. All statistical analyses were performed using GraphPad Prism.

3. Results

3.1. SRSF7 expression is significantly elevated in the lungs of IPF patients and BLM-induced experimental lung fibrosis model in mice

To elucidate the role of splicing factors in the progression of pulmonary fibrosis, we first examined the expression of transcripts encoding serine/arginine-rich proteins in the lungs of IPF patients. Our analysis revealed upregulation of SRSF1, SRSF2, SRSF7, and SRSF10 in IPF patients (Fig. 1A). Additionally, the expression of SRSF7 was also elevated in BLM-induced murine lung fibrosis (Supporting Information Fig. S1A and S1B). Given the critical role of lung fibroblasts in fibrosis, we used the Chan Zuckerberg Initiative online database to evaluate the prevalence and expression levels of SR proteins across different subtypes of human lung fibroblasts. Our results showed that SRSF7 was the most abundantly expressed SR protein in normal lung fibroblasts (Fig. 1B). Notably, we observed a significant positive correlation between SRSF7 expression and COL1A1, a key marker of fibrosis (Fig. 1C). Immunohistochemical analysis of lung tissues from IPF patients further demonstrated increased SRSF7 staining, predominantly in fibrotic regions (Fig. 1D).

We extended our investigation to the protein level and found that SRSF7 expression was significantly upregulated in lungs of IPF patients (Fig. 1E) and in mice following BLM administration (Fig. 1F). Furthermore, we analyzed single-cell RNA sequencing data to identify the expression of fibrosis-associated markers in SRSF7-positive fibroblasts. In GSE159354 (PF:IPF-4; CON:-Control-3), fibroblasts were first clustered with a resolution of 0.1, yielding 8 distinct cell subtypes (0−7). Fibroblasts with SRSF7 expression >0 were defined as $SRSF7^+$ fibroblasts. Genes were marked with an asterisk (*) if they were identified as markers for specific subtypes, based on a fibrosis-related gene set derived from the literature, which included 20 genes. Our analysis revealed the expression of fibrosis-associated markers such as ACTA2, FN1, COL1A1, and CD44 in $SRSF7^+$ fibroblasts (Fig. 1G). Moreover, we analyzed the single-cell dataset further and found that SRSF7 was predominantly expressed in fibroblasts and significantly upregulated in fibroblasts and myofibroblasts of IPF patients (Fig. S1C and S1D).

The subcellular localization of splicing factors is a critical determinant of their biological function. Our immunofluorescence data indicated that SRSF7 predominantly localized to the nucleus of lung fibroblasts after treatment with TGF-β1, suggesting that its role in regulating biological processes is likely mediated through the modulation of alternative splicing (Fig. 1H). Immunofluorescence assays further demonstrated that SRSF7 expression was specifically upregulated in S100A4-labeled fibroblasts after BLM treatment (Fig. 1I).

3.2. Overexpression of Srsf7 results in pulmonary fibrosis in mice

To elucidate the *in vivo* effects of *Srsf7*, we generated an adeno-associated virus (AAV) type 5 (AAV-*Srsf7*) and administered it *via* intratracheal injection. After 21 days of treatment, the mice were euthanized for subsequent evaluation. Utilizing micro-computed tomography (micro-CT), we observed that overexpression of *Srsf7* induced pulmonary fibrosis (Fig. 2A). Moreover, overexpression of *Srsf7* resulted in a significant reduction in lung function, including forced vital capacity (FVC), inspiratory capacity (IC), FEF 50% and dynamic compliance (Cdyn), along with changes in flow-volume loops (Fig. 2B). Histopathological examination following AAV-*Srsf7* treatment revealed increased collagen deposition and an expansion of fibrotic regions in the lungs of mice (Fig. 2C). H&E staining further demonstrated the destruction and thickening of alveolar septa after AAV-*Srsf7* administration (Fig. 2D).

Immunofluorescence and immunostaining further revealed that overexpression of *Srsf7* led to the upregulation of collagen I and α-SMA (Fig. 2E and F). In addition, qRT-PCR analysis demonstrated that overexpression of *Srsf7* significantly increased the mRNA levels of *Fn1, Col1a1, Col3a1*, and *Acta2* (Fig. 2G). Western blot results also confirmed that overexpression of *Srsf7* enhanced the expression of fibrosis-related proteins (Supporting Information Fig. S2). To further substantiate the *in vivo* function of fibroblasts with enhanced *Srsf7* expression, we isolated primary lung fibroblasts from the treated mice. Western blot analysis demonstrated that fibroblasts overexpressing *Srsf7* exhibited higher expression of fibrosis-related proteins (Fig. 2H). Consistently, both lung tissues and isolated primary lung fibroblasts from AAV-*Srsf7*-injected mice displayed increased mRNA expression levels of *Fn1*, *Col1a1*, *Col3α1* and *Acta2* (Fig. 2I).

3.3. SRSF7 promotes the activation of lung fibroblasts

Given the pronounced upregulation of *Srsf7* in the lung fibroblasts of BLM-treated mice, we further investigated the effect of SRSF7 on pulmonary fibroblasts. To determine its role in pulmonary fibrosis, we introduced *SRSF7* into the human fetal lung fibroblast cell line MRC-5 and human adult lung fibroblast HLFs (Supporting Information Figs. S3A and S4A). qRT-PCR analysis revealed that overexpression of *SRSF7* significantly increased the

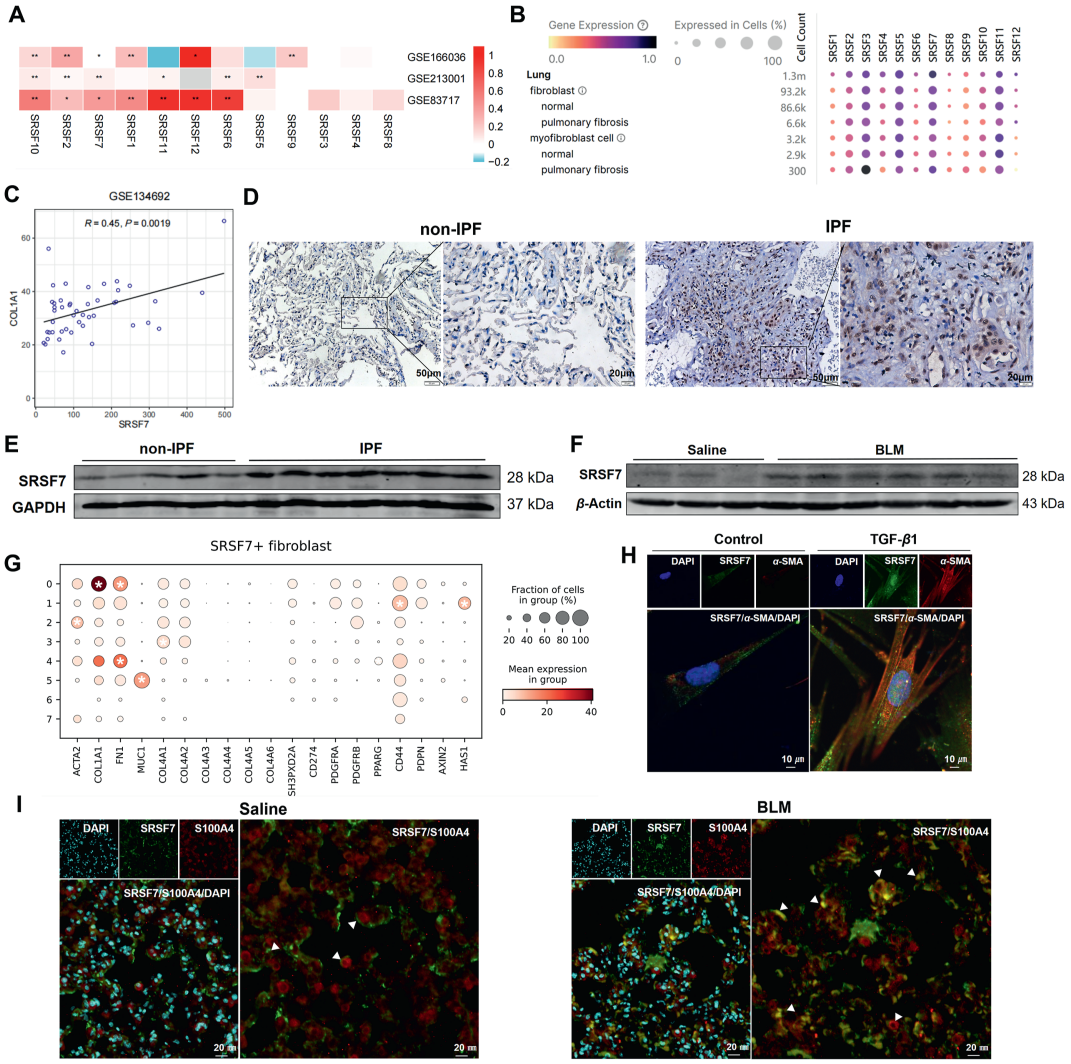

Figure 1 Increased expression of SRSF7 in lung fibroblasts during pulmonary fibrosis. (A) Heatmap of mRNA expression levels of serine/arginine-rich splicing factors in lung samples from GSE166036, GSE213001 and GSE83717. The color bars represent the range of $\log_2$FC values for each gene, with higher $\log_2$FC values shown in red and lower values in blue. $^*P < 0.05$, $^{**}P < 0.01$. (B) Single-cell RNA sequencing of annotated human lung fibrosis populations generated from Chan-Zuckerberg CELL by GENE Discover online database depicting relative expression of SRSF gene. Circle color denotes mean gene expression within each fibroblast subtype while circle size represents the proportion of each cell population expressing the indicated gene. (C) The Pearson's correlation analysis between the expression of COL1A1 and SRSF7 in the advanced IPF samples from GSE134692 dataset. The *X*-axis shows the FPKM-normalized expression values of the SRSF7 gene. The *Y*-axis shows the expression level of COL1A1. Pearson correlation (r) and *P*-value (P) are shown. (D) The IHC staining of SRSF7 in non-IPF and IPF patients. Non-IPF: $n = 6$, IPF: $n = 8$. (E) The protein expression of SRSF7 in lung tissues. Non-IPF: $n = 5$, IPF: $n = 7$. (F) The protein expression of SRSF7 in BLM treated mice. Saline: $n = 3$, BLM: $n = 6$. (G) In GSE159354, marker genes were identified using the rank_genes_groups function in Scanpy, with the wilcoxon test applied. Genes with a $\log_2\text{FC} \geq 4$ and $P < 0.05$ were considered markers and were marked with an asterisk. (H) Dual immunofluorescence in TGF-β1 treated MRC-5 cells. $n = 3$, scale bar = 10 μm. (I) Dual immunofluorescence of S100A4 (red) and SRSF7 (green) in frozen lung sections. $n = 3$, scale bar = 20 μm.

mRNA expression levels of *FN1, COL1A1*, *COL3A1*, and *ACTA2* in both MRC-5 cells and HLFs (Fig. 3A, Fig. S4A). Additionally, the expression of the fibrosis marker FN1 was notably enhanced in *SRSF7*-transfected MRC-5 cells (Fig. 3B). The cell contraction assay demonstrated that *SRSF7* enhanced the contractility of MRC-5 cells (Fig. 3C). Furthermore, *SRSF7* significantly promoted the proliferation and migration of fibroblasts (Fig. 3D, E, and Fig. S4E). Immunofluorescence experiments indicated that *SRSF7* overexpression facilitated the differentiation of fibroblasts into myofibroblasts (Fig. 3F).

Subsequently, we explored the effect of SRSF7 on TGF-β1-induced fibrogenesis. To investigate this, we designed four small interfering RNAs (siRNAs) to target *SRSF7* and suppress its expression in MRC-5 cells. qRT-PCR analysis demonstrated that two of the siRNAs effectively reduced *SRSF7* expression in both MRC-5 cells and HLFs (Figs. S3A and S4C). As shown in Fig. 3G and Fig. S4C, silencing of *SRSF7* mitigated the TGF-β1-induced upregulation of *FN1, COL1A1, COL3A1,* and *ACTA2*. Western blot analysis further confirmed that *SRSF7* knockdown inhibited the TGF-β1-induced increase in FN1 and α-SMA protein

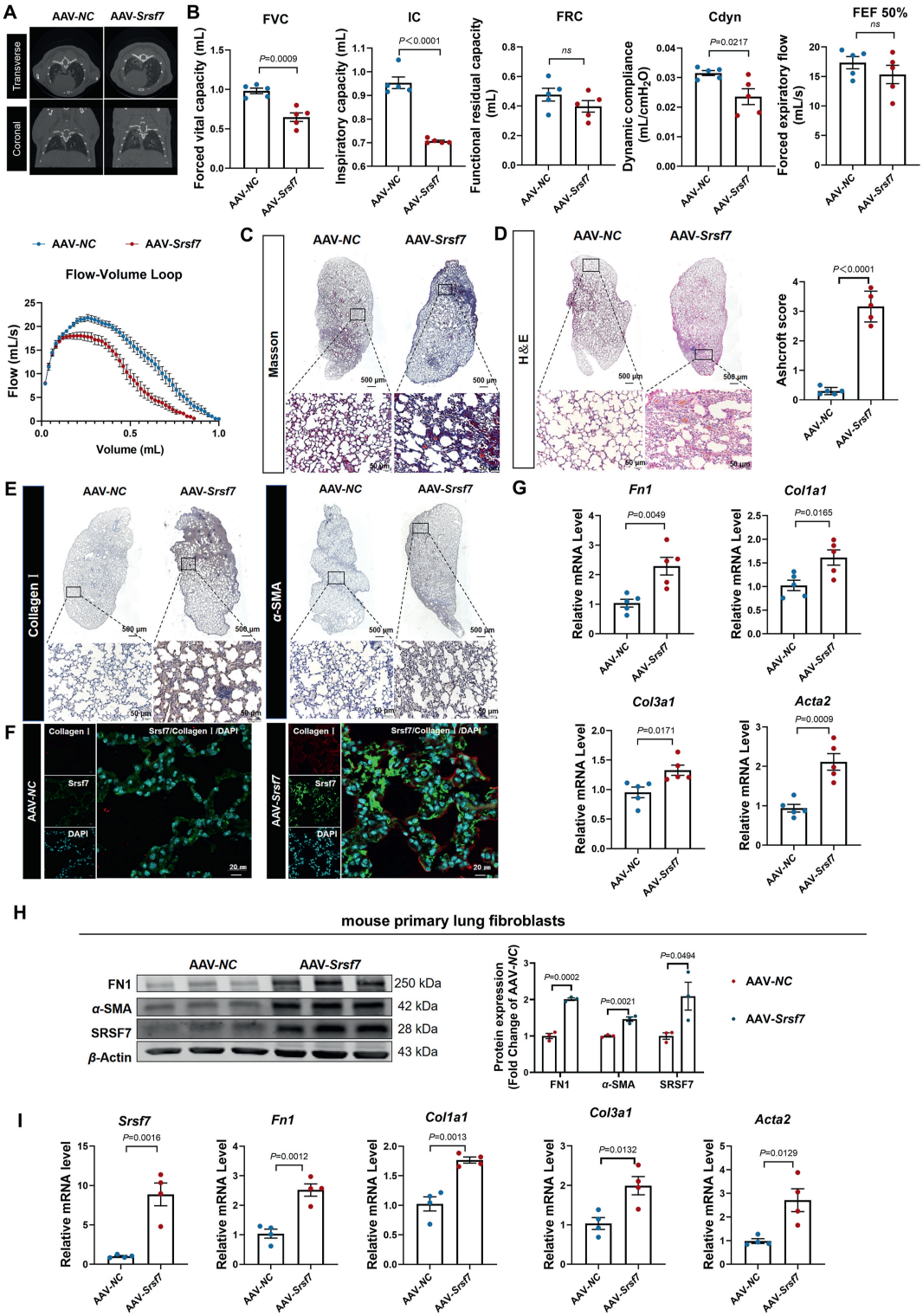

Figure 2 Overexpression of SRSF7 led to pulmonary function decline. (A) micro-CT was used to observe the fibrosis of mouse lung; $n = 5$. (B) FVC, IC, FRC, Cdyn, FEF 50% and Flow-volume loop were detected in mice treated with AAV-*NC* and AAV-*Srsf7*; $n = 5$. (C) Masson staining was used to evaluate the content of collagen in lung tissues; $n = 4$, scale bar = 500 μm. (D) The alveoli structure detected by H&E staining and the degree of interstitial lung fibrosis were determined by using a predetermined numerical scale of 0−8, based on the Ashcroft scoring method; $n = 5$, scale bar = 500 μm. (E, F) Collagen I and α-SMA were stained by IHC (n = 3, scale bar = 500 μm) and immunofluorescence staining (n = 4, scale bar = 20 μm). (G) The mRNA expression of *Fn1, Col1α1, Col3α1* and *Acta2* in mice treated with AAV-*NC* and AAV-*Srsf7*; $n = 5$. (H) The protein expression of FN1, α-SMA and SRSF7 in the lung fibroblasts of mice. (I) The mRNA expression of fibrosis markers in mice treated with AAV-*NC* and AAV-*Srsf7*; $n = 4$. Data are presented as mean ± SEM; ns, no significance.

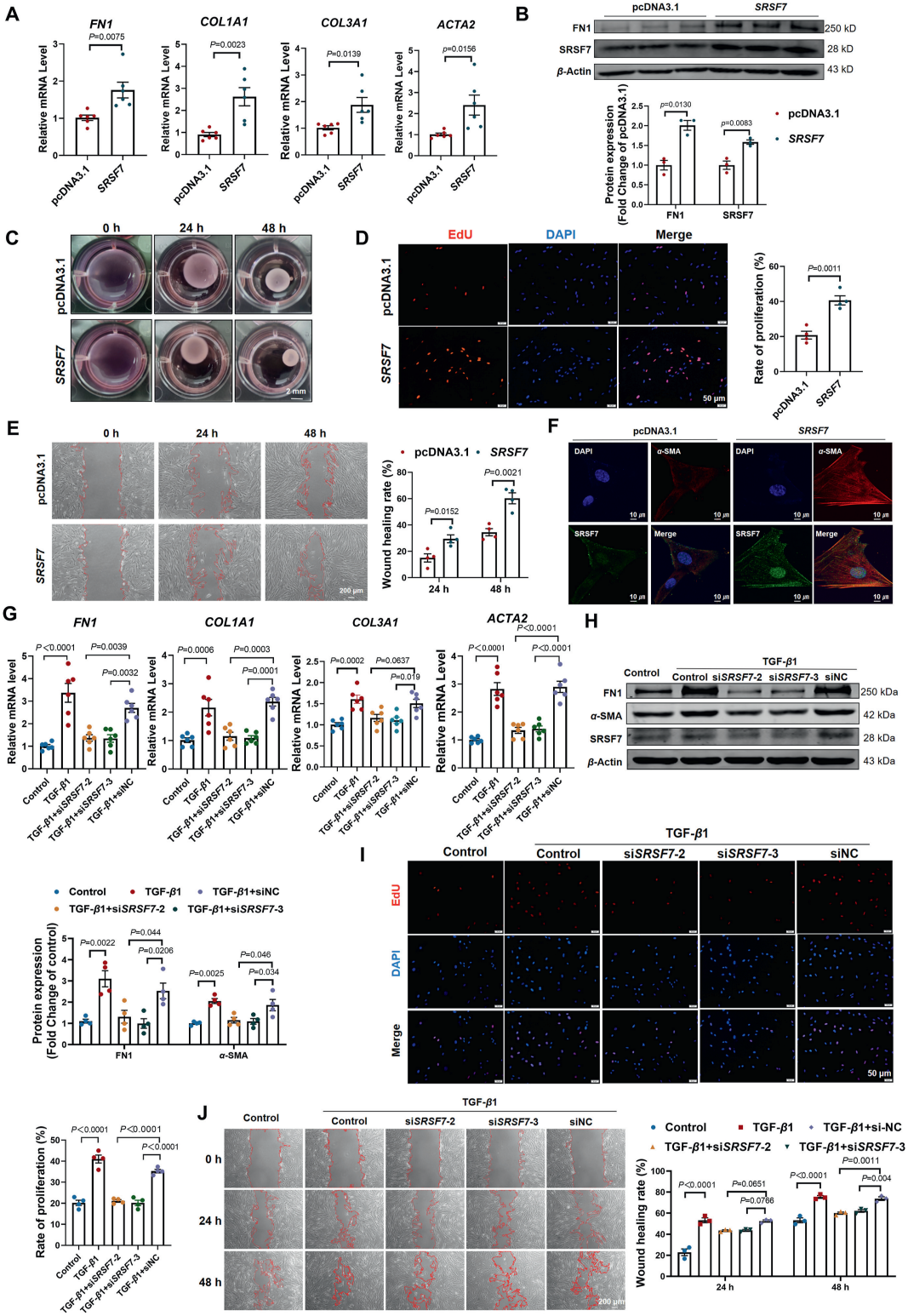

Figure 3 SRSF7 promotes fibroblast activation and fibrogenesis. (A) The mRNA expression of fibrosis related genes after MRC-5 cells transfected with *SRSF7*; $n = 6$. (B) Western blot demonstrated increased expression level of Fn1 in *SRSF7* transfected MRC-5 cells; $n = 3$. (C) Relative quantification of the collagen contraction area after transfected with *SRSF7*; $n = 3$. (D, E) EdU assay (scale bar = 50 μm, $n = 4$) and wound healing experiment (scale bar = 200 μm, $n = 4$) indicated that transfected with *SRSF7* promoted the proliferation and migration of MRC-5. (F) Overexpression of *SRSF7* promoted the fibroblast-myofibroblast transformation of MRC-5 cells; $n = 3$, scale bar = 10 μm. (G) qRT-PCR analysis demonstrating the relative expression of *FN1*, *COL1A1*, *COL3A1* and *ACTA2* in TGF-β1-induced MRC-5 cells transfected with or without si-*SRSF7*; $n = 6$. (H) Western blot showed that the si-*SRSF7* abrogated the upregulation of fibrotic proteins in MRC-5 cells induced by TGF-β1; $n = 4$. (I, J) EdU (scale bar = 50 μm, $n = 4$) and wound healing assays (scale bar = 200 μm, $n = 3$) indicated that si-*SRSF7* inhibited the proliferation and migration of MRC-5 cells. Data are presented as mean ± SEM.

expression (Fig. 3H). Moreover, the cell contraction assay revealed that *SRSF7* silencing significantly reduced the contractility enhancement induced by TGF-β1 in MRC-5 cells (Fig. S3B). Consistently, silencing of *SRSF7* also dampened the proliferation and migration of fibroblasts driven by TGF-β1 (Fig. 3I, J, and Fig. S4F). Immunofluorescence experiments further substantiated the role of *SRSF7* silencing in curtailing the formation of myofibroblasts (Fig. S3C).

3.4. Global landscape of the SRSF7-affected alternative splicing and gene expression in MRC-5 cells

As previously discussed, the subcellular localization of SRSF7 is pivotal in determining its mechanism of action. The pro-fibrotic effects observed in SRSF7-overexpressing mice may be attributed to its role in regulating alternative splicing. To identify SRSF7-regulated AS events involved in lung fibrosis, we conducted high-throughput RNA sequencing (RNA-seq) on MRC-5 cells transfected with *SRSF7*. Illumina sequencing and SMRT sequencing results uncovered a plethora of differentially expressed genes (DEGs) and AS events that are potentially modulated by *SRSF7* in fibroblasts. Using DESeq2 for analysis, we identified 950 DEGs between the *SRSF7* overexpression group and the pcDNA3.1 control group ($|\log2FC| > 1$, $P < 0.05$) (Fig. 4A). Gene Ontology (GO) analysis indicated significant enrichment of genes affected by *SRSF7* overexpression in pathways related to TGF-β signaling, extracellular matrix (ECM)-receptor interaction, and spliceosome function (Fig. 4B). Complementary pathway enrichment analysis *via* Gene Set Enrichment Analysis (GSEA) revealed an enrichment of U2 small nuclear ribonucleoprotein (snRNP) and splicing complex-associated genes following SRSF7 overexpression (Fig. 4C).

Employing the rMATs software, we systematically identified exon-centric differential splicing events across a vast genomic range. This approach yielded a comprehensive dataset of both annotated and novel splice junctions, encompassing 1985 AS events across the five major AS patterns (Fig. 4D). To identify biological processes associated with these transcriptome changes, Gene Ontology (GO) enrichment analysis was performed. The results demonstrated that *SRSF7* was significantly involved in alternative splicing (Fig. S5A). To validate the accuracy of our RNA-seq results on AS events, we subsequently verified specific AS events by qRT-PCR (Fig. S5B). Notably, we identified a consistent SRSF7-regulated AS event in the pyruvate kinase M (*PKM*) gene in both MRC-5 cells and IPF patients. Our findings revealed that *PKM* is spliced by SRSF7 in both MRC-5 cells and IPF patient samples (Fig. 4E). Furthermore, overexpression of SRSF7 in lung fibroblasts promoted the exclusion of *PKM* exon 2, resulting in the exon 2 skipping (*PKMΔE2*) isoform (Fig. 4F and Fig. S4B). qRT-PCR results also demonstrated that TGF-β1 induced *PKM* exon 2 skipping in lung fibroblasts, an effect that was attenuated by *SRSF7* knockdown (Fig. 4G and Fig. S4D). To extend our findings *in vivo*, we isolated mouse primary lung fibroblasts and assessed the impact of *SRSF7* overexpression on *PKM* alternative splicing. As shown in Fig. 4H, overexpression of *SRSF7 in vivo* also promoted *PKM* exon 2 skipping. To further elucidate the molecular mechanism underlying SRSF7 in *PKM* splicing, we constructed a minigene encompassing a fragment of the *PKM* gene, including the region flanking exon 2 (200 nt upstream and 200 nt downstream) along with adjacent constitutive exons. Our analysis of protein-RNA interactions identified multiple binding sites between SRSF7 and *PKM* (Fig. S5C). Introducing mutations into the binding sites within the highest affinity region (designated minigene-mut) significantly impaired SRSF7-mediated splicing of *PKM*. To explore the specific binding site for SRSF7 on the *PKM* pre-mRNA, we conducted site-directed mutagenesis of the polypyrimidine tract within the original *PKM*-minigene plasmid vector. qRT-PCR results indicated that SRSF7 could mediate the splicing of exogenous PKM fragments, but this activity was abrogated upon transfection with the minigene-mut construct (Fig. 4I). Additionally, we constructed the functional domain plasmid of SRSF7 and demonstrated that the absence of any domain resulted in the loss of SRSF7 regulatory effect on the alternative splicing of *PKM* (Fig. 4J). Furthermore, RNA immunoprecipitation (RIP) assays indicated robust interactions between SRSF7 and *PKM*, as well as snRNA components of the early spliceosome (U1/U2), in MRC-5 cells (Fig. 4K and L). Importantly, we found that overexpression of SRSF7 had no significant effect on PKM protein expression (Fig. S5D). Together, these results suggest that SRSF7 can directly bind to *PKM* through the spliceosome to regulate the occurrence of its alternative splicing events.

3.5. PKM△E2 promotes fibrogenesis in MRC-5 cells by accelerating glycolysis

To elucidate the distinct functional roles of the two splicing isoforms of *PKM*, we constructed plasmids encoding the respective transcripts. We then assessed the effects of these isoforms on the expression of fibrosis-related markers. The results demonstrated that the *PKMΔE2* isoform induced significantly higher expression of *FN1*, *COL1A1*, and *ACTA2* compared to the full-length *PKM* isoform (Fig. 5A). Western blot analysis further confirmed that overexpression of *PKMΔE2* increased the protein levels of FN1 and α-SMA compared to the full-length *PKM* (Fig. 5B). Concurrently, forced expression of *PKMΔE2* promoted the proliferation and migration of MRC-5 cells (Fig. 5C and D). Moreover, MRC-5 cells transfected with *PKMΔE2* exhibited increased contractility compared to those transfected with the full-length *PKM* (Fig. 5E).

Given the role of PKM as a pyruvate kinase catalyzing the final step of glycolysis, we utilized a pyruvate kinase activity assay kit to compare the enzymatic activities of the two *PKM* isoforms. The results revealed that *PKMΔE2* exhibited significantly higher kinase activity compared to the full-length *PKM* isoform (Fig. 5F). To further investigate the metabolic consequences of these differences, we measured glucose consumption and lactate production in fibroblasts expressing the two splicing isoforms. Notably, fibroblasts transfected with *PKMΔE2* displayed elevated lactate levels compared to those transfected with full-length *PKM* (Fig. 5F). To determine whether the profibrotic function of *PKMΔE2* is linked to glycolytic dysregulation, we employed the Seahorse XFe96 Extracellular Flux Analyzer to assess the extracellular acidification rate (ECAR), a key indicator of lactate production. As shown in Fig. 5G, enhanced expression of *PKMΔE2* led to an early and sustained increase in ECAR, indicative of enhanced glycolysis in MRC-5 cells. Additionally, the oxygen consumption rate (OCR), which reflects mitochondrial respiration, exhibited a consistent upward trend following transfection with both the *PKM* and *PKMΔE2* isoforms (Fig. 5H). Collectively, these results suggest that *PKMΔE2* promotes glycolysis, thereby driving fibrogenesis in fibroblasts.

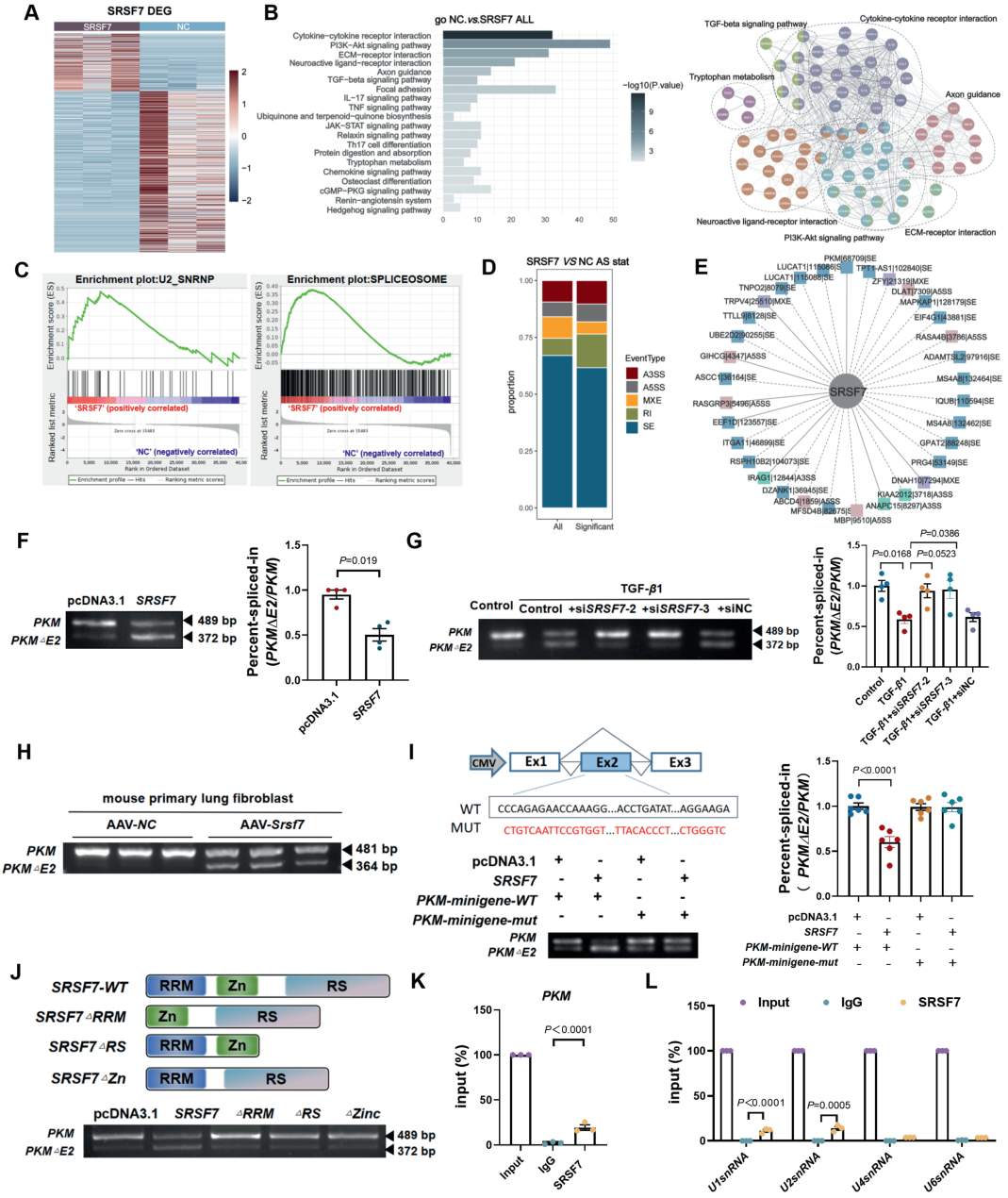

Figure 4 SRSF7 is able to bind to and regulate the alternative splicing of PKM. (A) Heatmap illustrating differentially expressed genes. Red represents up-regulated, and blue represents down-regulated. In the heatmap, red indicates high gene expression, while blue represents low gene expression. The color bars display the scale of values for each gene, ranging from −2 to 2 as shown on the right. (B) GO enrichment analysis regulated by overexpression of *SRSF7*. (C) GSEA showed that U2 SnRNP and spliceosome related genes were significantly enriched after overexpression of *SRSF7*. (D) The differentially alternative splicing genes regulated by SRSF7 were mainly enriched in exon skipped events. (E) Prediction of SRSF7 regulated alternative splicing genes overlap in MRC-5 and IPF patients. (F) SRSF7 enhanced the alternative splicing of *PKM* exon 2; $n = 4$. (G) Silencing SRSF7 can reduce the skipping of *PKM* exon 2 induced by TGF-β1; $n = 4$. (H) Lung fibroblasts were isolated from mice to detect the alternative splicing events of *PKM*. (I) Minigene reporters of *PKM* were introduced into SRSF7-overexpression cells; $n = 6$. (J) Deficiency of the SRSF7 function domain on alternative splicing of *PKM* exon 2. (K) RIP experiments were performed to detect the binding relationship between SRSF7 and *PKM*; $n = 3$. (L) The effect of SRSF7 on the ability of binding with snRNAs was investigated by the RIP experiment; $n = 3$. Data are presented as mean ± SEM.

3.6. PKMΔE2 is necessary for the pro-fibrotic effect of SRSF7

To examine whether *PKMΔE2* mediates the regulatory effect of SRSF7 on lung fibrosis, we transfected TGF-β1-treated MRC-5 cells with a plasmid for *PKMΔE2* overexpression and siRNA targeting *SRSF7*. qRT-PCR analysis revealed that enhanced expression of *PKMΔE2* alleviated the *SRSF7* knockdown-induced reduction in *FN1*, *COL1A1*, *COL3A1*, and *ACTA2* levels in TGF-β1-treated MRC-5 cells (Fig. 6A). Additionally, overexpression of *PKMΔE2* restored cell contractility, which was previously reduced

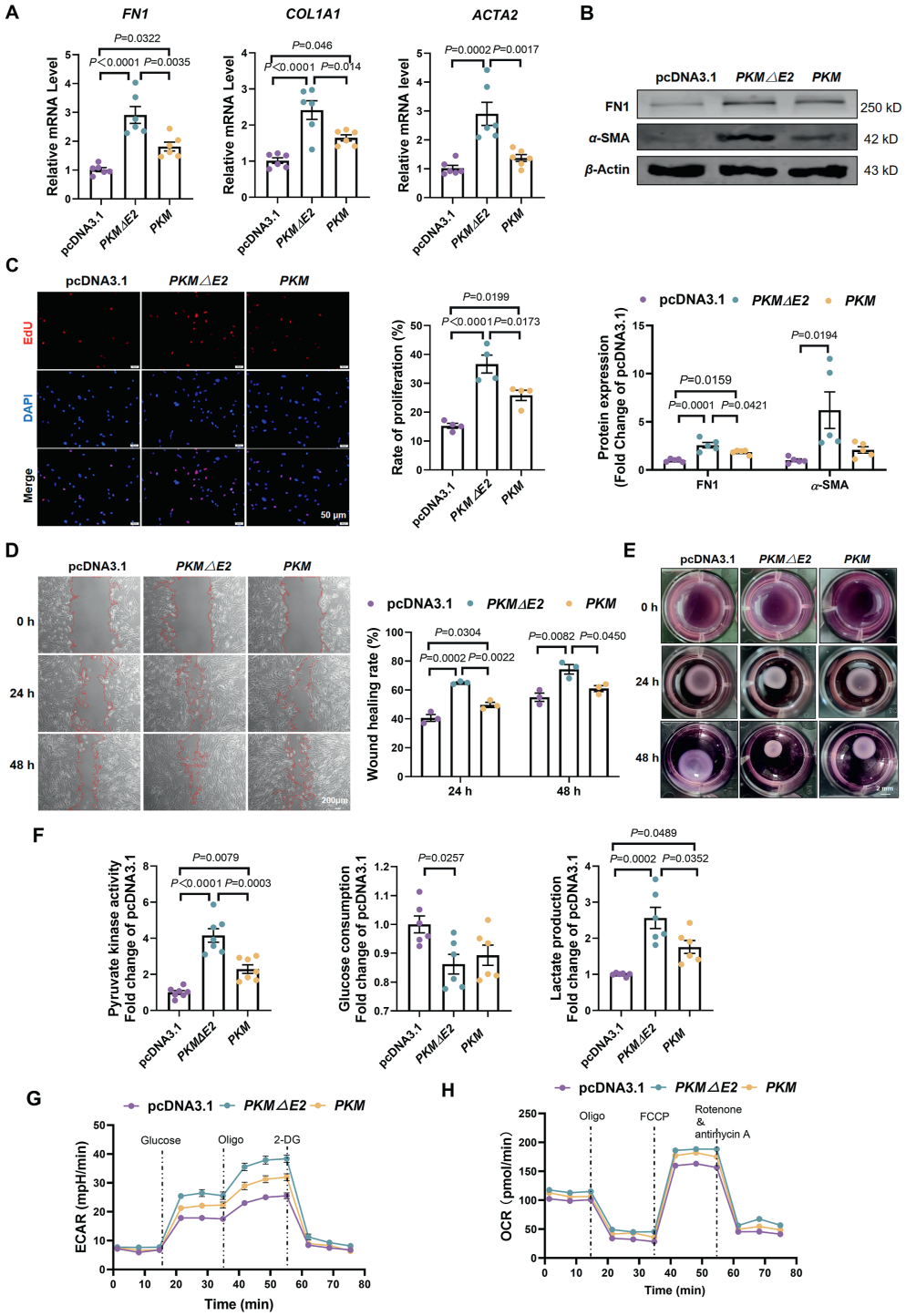

Figure 5 *PKMΔE2* isoform promotes fibroblasts activation. (A) The mRNA expression of fibrosis related genes; $n = 6$. (B) Western blot suggested that *PKM* isoforms promote the expression of FN1 and α-SMA; $n = 5$. (C, D) EdU (scale bar = 50 μm, $n = 4$) and wound healing assays (scale bar = 200 μm, $n = 3$) indicated that *PKM* isoforms can promote the cell proliferation and migration. (E) Relative quantification of the collagen contraction area after overexpression of *PKM* isoforms; $n = 3$. (F) Overexpression of *PKMΔE2* increased the pruvate activity and lactic acid content compared with *PKM*. (G, H) MRC-5 cells were seeded in Seahorse XF-96 cell culture microplates. The cells were transfected with *PKM* and *PKMΔE2*, followed by sequential treatments with oligomycin (Oligo) and FCCP. Real-time ECAR and OCR were recorded. Data are presented as mean ± SEM.

by *SRSF7* silencing in TGF-β1-treated MRC-5 cells (Fig. 6B). As shown in Fig. 6C, overexpression of *PKMΔE2* reversed the inhibition of fibroblast-to-myofibroblast transition induced by si*SRSF7* in TGF-β1-treated MRC-5 cells. Furthermore, silencing *SRSF7* attenuated the TGF-β1-induced proliferation and migration in MRC-5 cells, an effect that was abolished by concurrent overexpression of *PKMΔE2*, indicating that the anti-fibrotic action of *SRSF7* knockdown was counteracted by *PKMΔE2* (Fig. 6D and E).

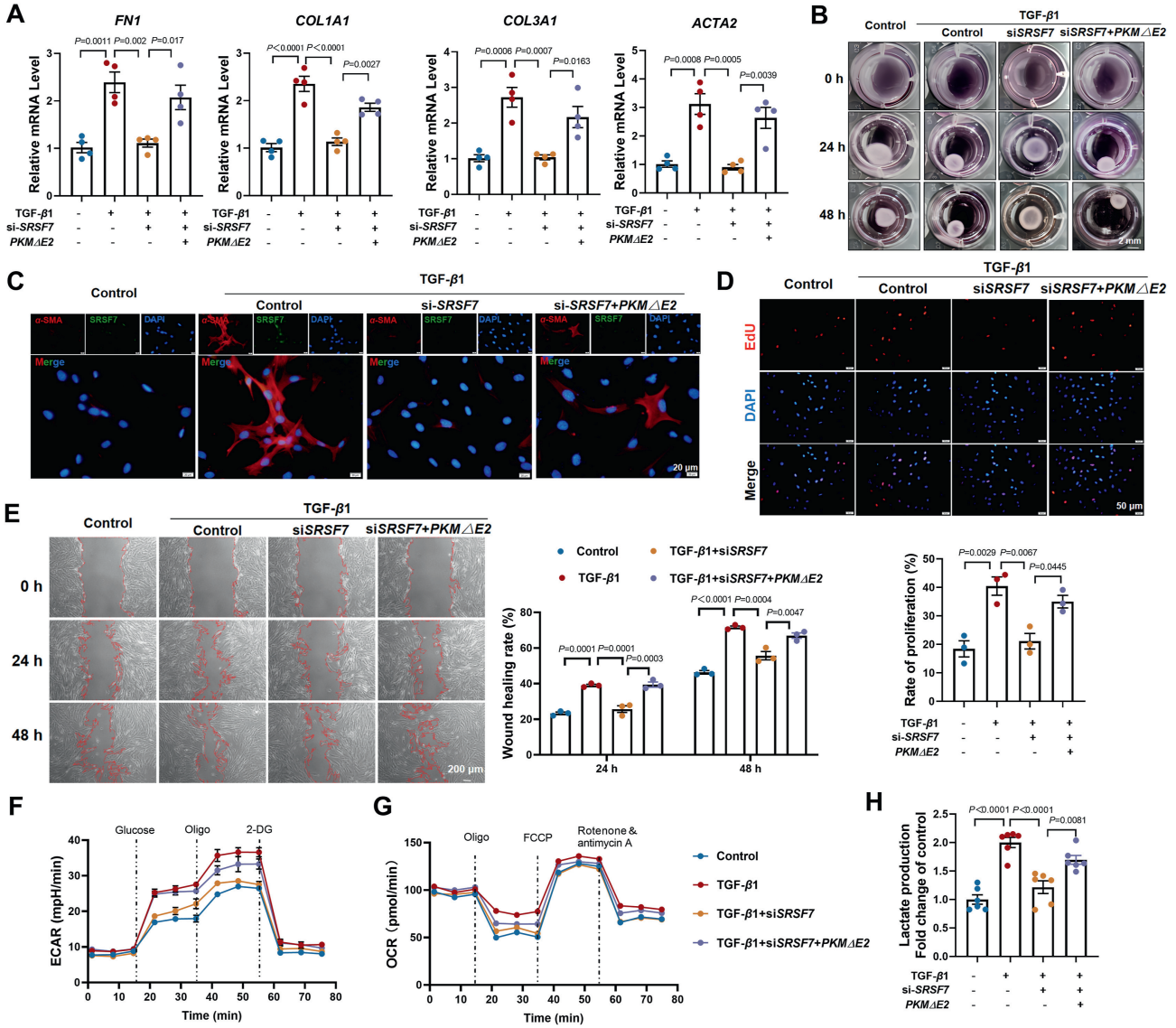

Figure 6 Silencing *SRSF7* alleviates fibrogenesis by inhibiting the expression of *PKMΔE2* isoform. (A) The mRNA expression of *FN1*, *COL1A1*, *COL3A1* and *ACTA2*; $n = 4$. (B) Relative quantification of the collagen contraction area in MRC-5 cells; $n = 3$. (C) Immunofluorescence showed the fibroblasts transformation in MRC-5; $n = 3$, scale bar = 20 μm. (D, E) EdU (scale bar = 50 μm, $n = 3$) and wound healing assays (scale bar = 200 μm, $n = 3$) indicated that overexpression of *PKMΔE2* promoted the cell proliferation and migration reduced by si*SRSF7*. (F, G) Real-time ECAR and OCR were recorded in the MRC-5 transfected with si*SRSF7* and *PKMΔE2* after treatment with TGF-β1. (H) The lactic acid content of MRC-5 cells, $n = 6$. Data are presented as mean ± SEM.

The Seahorse respiration assay demonstrated that *PKMΔE2* contributed to glycolytic dysregulation (Fig. 6F and G). Moreover, the measurement of lactate production in fibroblasts showed that glucose consumption was significantly higher in the *PKMΔE2* group compared to MRC-5 cells transfected solely with si*SRSF7* (Fig. 6H). Collectively, these findings suggest that *PKMΔE2* acts as a downstream effector of *SRSF7*, mediating glycolytic dysregulation and contributing to lung fibrosis in MRC-5 cells.

3.7. Fibroblasts-specific knockout of Srsf7 alleviates pulmonary fibrosis in mice

To investigate the function of Srsf7 *in vivo*, we developed transgenic mice with fibroblast-specific *SRSF7* deficiency (*Srsf7*$^{flox/flox}$; *Col1a2*-CreERT), hereafter referred to as *Srsf7*-cKO mice. In these mice, exon 3 of the *Srsf7* gene was precisely excised (Supporting Information Fig. S6A). The successful integration of LoxP sites and the *Col1a2*-CreERT construct was verified through mouse tail genomic identification (Fig. S6B). Mice were administered tamoxifen intraperitoneally at a dosage of 80 mg/kg for one week to induce recombination prior to BLM challenge, allowing evaluation of the potential effect of *Srsf7* deficiency on lung fibrosis (Fig. 7A). Micro-CT assessment indicated that *Srsf7*-deficiency mice exhibited diminished BLM-induced pulmonary fibrosis (Fig. 7B). Additionally, pulmonary function parameters, including forced vital capacity (FVC), inspiratory capacity (IC), functional residual capacity (FRC), and dynamic compliance (Cdyn), as well as flow-volume loops, showed improvement in *Srsf7*-cKO mice (Fig. 7C and D). Histopathological examination revealed a reduction in collagen deposition and fibrotic area in *Srsf7*-cKO mice (Fig. 7E and F). The hydroxyproline content assay demonstrated that *Srsf7* deficiency led to a significant

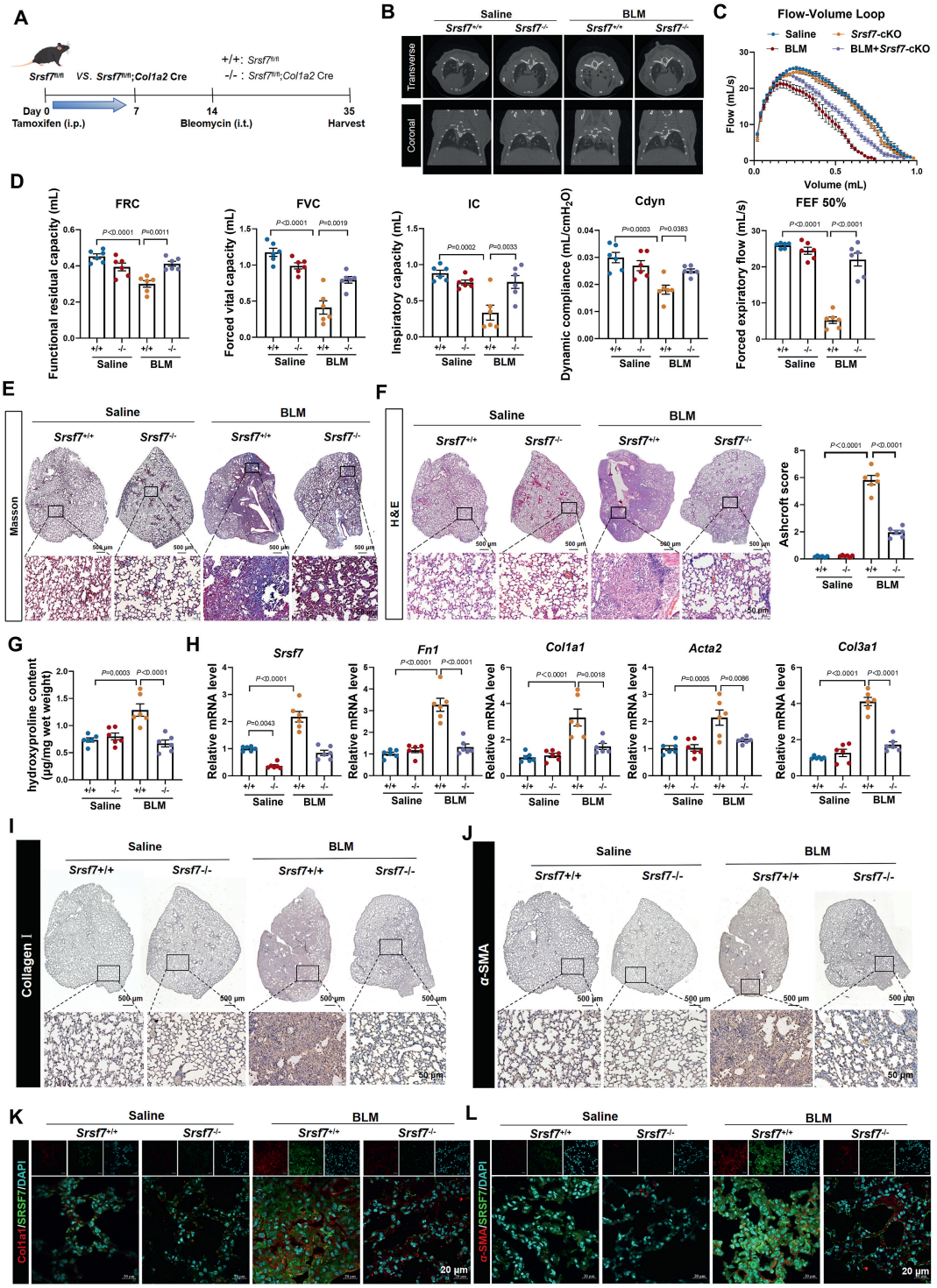

Figure 7 *Srsf7* deficiency attenuates BLM-induced experimental lung fibrosis in mice. (A) Diagram of the animal experimental model of *Srsf7*-cKO. (B) Representative micro-CT images showed the lung fibrosis of *Srsf7*-cKO mice treated with bleomycin for 21 days; $n = 4$. (C, D) FRC, FVC, IC, FEF50%, Cdyn and F−V Loop were detected in $Srsf7^{fl/fl}$ or *Srsf7*-cKO mice treated with saline or bleomycin for 21 days; $n = 6$. (E) Masson and (F) H&E staining were used to evaluate the content of collagen in lung tissues; $n = 6$, scale bar = 500 μm. (G) The hydroxyproline content detection in lung tissues was confirmed by hydroxyproline detection kit; $n = 6$. (H) qRT-PCR was used to determine the mRNA level of *Srsf7*, *Fn1*, *Acta2*, *Col1a1 and Col3a1*; $n = 6$. (I, J) IHC ($n = 3$, scale bar = 500 μm) and (K, L) immunofluorescence staining ($n = 4$, scale bar = 20 μm) were used to evaluate the expression of Collagen I and α-SMA in lung tissues. Data are presented as mean ± SEM.

decrease in collagen deposition (Fig. 7G). qRT-PCR results showed that the mRNA levels of *Col1a1*, *Col3a1*, *Fn1*, and *Acta2* were also attenuated in the lungs of Srsf7-deficient mice (Fig. 7H). Immunohistochemistry and immunofluorescence analyses further substantiated the downregulation of Collagen I and α-SMA in the lungs of *Srsf7*-cKO mice (Fig. 7I–L). Consistent with these results, Western blot analysis exhibited a reduction of FN1 and α-SMA in the *Srsf7*-cKO mice (Fig. S6C). PCR results also demonstrated that deficiency of *Srsf7* reduced exon 2 skipping compared to BLM treatment alone (Fig. S6D).

3.8. Lomitapide inhibits SRSF7 expression to alleviate experimental lung fibrosis and improve lung function in mice

To further evaluate the therapeutic potential of targeting SRSF7 for the treatment of lung fibrosis, we conducted a comprehensive chemical screen to identify SRSF7 inhibitors from a diverse drug library (https://www.selleckchem.com). We employed an EGFP-*SRSF7* plasmid-transfected HEK-293T cell model and incubated these cells with a collection of 3105 distinct compounds for 12 h at a concentration of 2 μmol/L. After quantitative analysis of fluorescence signals, we identified 10 compounds that effectively reduced the expression of EGFP-*SRSF7* (Supporting Information Fig. S7A and S7B). Subsequently, we separately administered these compounds to MRC-5 cells treated with TGF-β1 to assess their efficacy. Among the identified candidates, Lomitapide, a novel lipid-lowering agent initially developed for the treatment of homozygous familial hypercholesterolemia (HoFH), emerged as a potent suppressor of *SRSF7* expression. To further investigate its mechanism, we performed a computational prediction of the interaction between Lomitapide and SRSF7 using AutoDock Vina (Fig. 8A). This discovery prompted us to explore the therapeutic potential of Lomitapide in the context of pulmonary fibrosis (Fig. 8B).

Micro-CT assessment revealed that Lomitapide treatment significantly mitigated BLM-induced pulmonary fibrosis in mice (Fig. 8C). Pulmonary function tests demonstrated improvements in vital lung functions, with increases in FVC, IC, FRC and Cdyn, as well as restoration of normal flow-volume loops in treated mice (Fig. 8D and Fig. S7C). As shown in Fig. 8E and F, Lomitapide reduced extracellular matrix deposition, collagen formation, and myofibroblast activation, which are characteristic of BLM-induced lung injury. The hydroxyproline content assay revealed a significant reduction in collagen deposition due to Lomitapide treatment (Fig. 8G). Furthermore, qRT-PCR results showed decreased mRNA expression levels of *Col1a1, Col3a1, Fn1* and *Acta2* in the lungs of Lomitapide-treated mice (Fig. 8H). Immunohistochemistry and immunofluorescence analyses corroborated these findings, demonstrating diminished expression of Collagen I and α-SMA in the lungs of Lomitapide-treated mice (Fig. 8I–L). Western blot analysis also confirmed that Lomitapide reduced the expression of FN1 and α-SMA in BLM-treated mice (Fig. S7D). We also performed PCR experiments to determine the effect of *Srsf7* on PKM alternative splicing *in vivo*. The results showed that Lomitapide treatment significantly reduced exon 2 skipping compared to BLM treatment alone (Fig. S7E).

4. Discussion

In the present study, we screened differentially expressed splicing factors in pulmonary fibrosis and characterized the underlying mechanism of SRSF7 in IPF. We identified, for the first time, increased expression of SRSF7 in the lung tissue of IPF patients and BLM-treated mice. Subsequent experimental results demonstrated that overexpression of SRSF7 in MRC-5 cells promoted fibrogenesis by binding to and regulating the alternative splicing of *PKM*, thereby mediating dysregulation of glycolysis. Furthermore, we screened an FDA-approved drug library using SRSF7 as a drug target and confirmed its anti-fibrotic function in mice.

The SR family consists of 12 highly conserved splicing factors and is involved in nearly all aspects of RNA synthesis[29]. Despite their broad implications, studies on SR family members in fibrosis-related diseases remain limited. Previous research has reported that SRSF7 plays a critical role in cellular senescence by generating MDM2 variants and establishing age-dependent alternative splicing in mice[25]. Additionally, SRSF7 has been positively correlated with multiple immune checkpoint genes and has emerged as a promising prognostic biomarker in hepatocellular carcinoma, where it is associated with immune infiltration[30]. Overexpression of SRSF7 has also been observed in colon and lung cancer tissues, suggesting its potential as a therapeutic target for these malignancies[31]. One of the underlying mechanisms of SRSF7 involves its role in modulating 3′UTR length through the suppression or activation of proximal polyadenylation sites and regulation of CFIm levels[32]. In the present study, our data have revealed a novel function of SRSF7 in the lung and provided evidence that SRSF7 regulates alternative splicing within fibroblasts.

A growing understanding of IPF has highlighted the importance of the activation and differentiation of lung fibroblasts as key drivers of fibrosis. With the recent development of single-cell sequencing assays for the detection of IPF, we analyzed the expression of SRSF7 across different cell types. Our results indicated that SRSF7 was predominantly enriched in fibroblasts and myofibroblasts from IPF patients, suggesting its potential as a candidate target for pharmacotherapy. Additionally, the mRNA expression of *SRSF7* in lung tissue was positively correlated with the expression of *COL1A1*, a hallmark of IPF. To further investigate the function of SRSF7 *in vivo*, mice were subjected to intratracheal injection with AAV-*Srsf7*. The *in vivo* results confirmed that overexpression of *Srsf7* spontaneously induced mild pulmonary fibrosis. Furthermore, to explore the underlying mechanism of SRSF7, we utilized human fetal lung fibroblasts in our experimental studies.

SR proteins regulate gene expression levels through multiple pathways, including mRNA export, mRNA stability, and mRNA translation, in addition to modulating transcriptional length and sequence composition, depending on their diverse subcellular localizations in mammalian cells[33]. These proteins are characterized by the presence of an RS domain (containing arginine [R] and serine [S] amino acids) at the C-terminus and an RRM domain (RNA recognition motif) at the N-terminus. In general, the RRM domain facilitates RNA recognition, while the RS domain is involved in protein–protein and protein-RNA interactions[34]. Notably, SRSF7 is unique among SR family members as the only one containing a zinc finger domain, enabling it to shuttle between the nucleus and cytoplasm[35]. To further investigate the subcellular localization of SRSF7 during fibroblast activation, we analyzed its distribution in response to TGF-β1. Our results revealed that SRSF7 accumulated in the nucleus following TGF-β1 stimulation, suggesting that its role in promoting fibroblast activation is primarily mediated through the regulation of alternative splicing. In the nucleus, SR proteins bind to pre-mRNA in a sequence-specific manner, recruiting spliceosomes to precisely excise introns and produce mature mRNA[36]. In our study, we utilized both Illumina

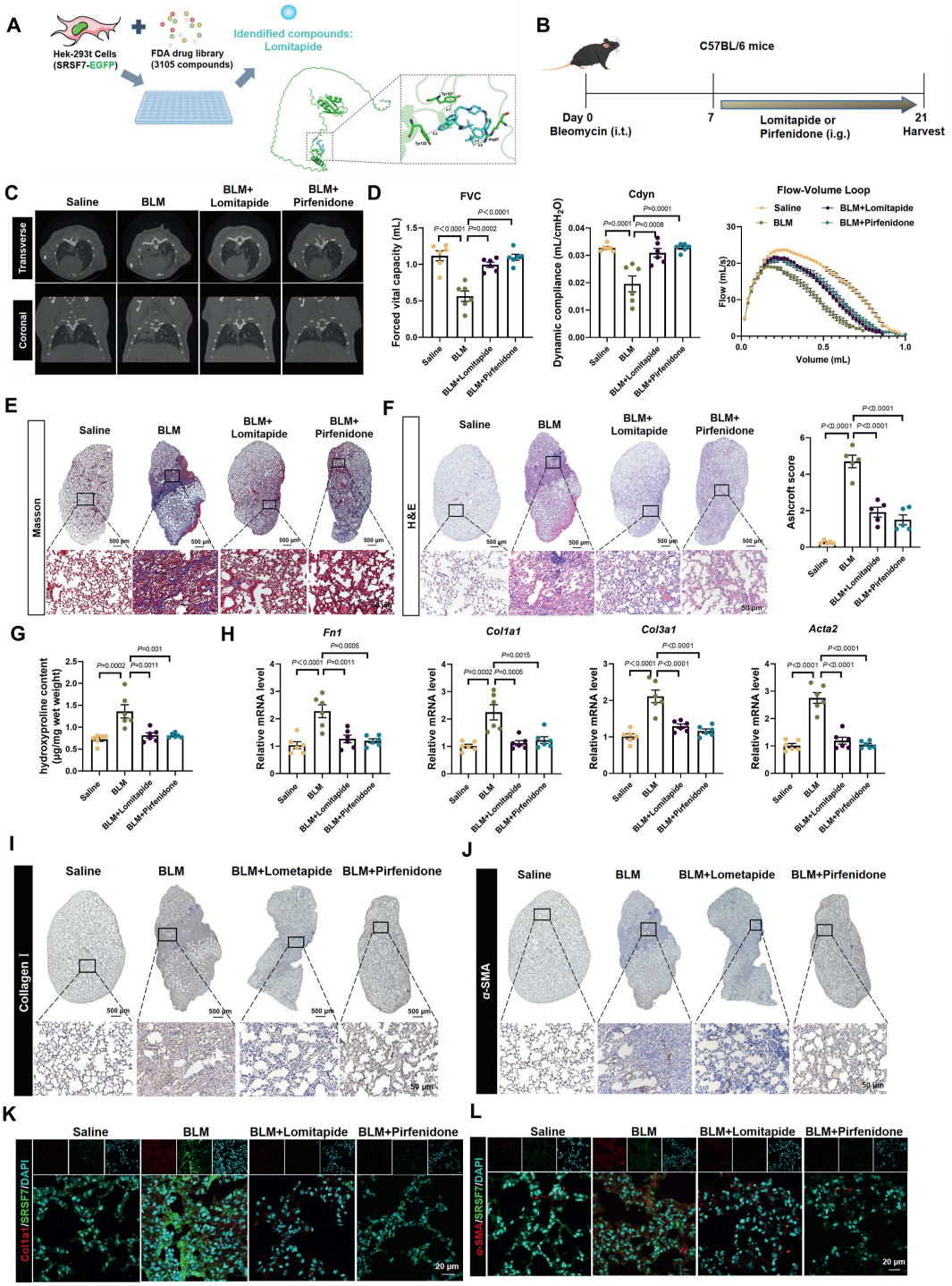

Figure 8 Lomitapide inhibits SRSF7 expression to improve lung fibrosis and lung function in mice. (A) Chemical screen to systematically identify inhibitors of SRSF7 and prediction of Drug−Protein Interaction Networks from the Integration of SRSF7 Sequences and Lomitapide Chemical Structures (right panel). (B) Experimental protocol of lomitapide in BLM treated mice. (C) Representative micro-CT images showed the lung fibrosis of lomitapide treated mice; $n = 4$. (D) FVC, Cdyn and F−V Loop were detected in mice treated with lomitapide or pirfenidone; $n = 6$. (E) Masson and (F) H&E staining were used to evaluate the content of collagen in lung tissues; $n = 5$, scale bar = 500 μm. (G) The hyroxyproline content detection in lung tissues was confirmed by hydroxyproline detection kit; $n = 6$. (H) qRT-PCR was used to determine the mRNA level of *Fn1*, *Acta2*, *Col1a1* and *Col3a1* in lomitapide or pirfenidone treated mice; $n = 6$. (I, J) IHC ($n = 4$, scale bar = 500 μm) and (K, L) immunofluorescence staining ($n = 3$, scale bar = 20 μm) were used to evaluate the expression of Collagen I and α-SMA in lung tissues. Data are presented as mean ± SEM.

and PacBio SMRT sequencing to identify the alternative splicing (AS) events potentially regulated by SRSF7. Our findings demonstrated that SRSF7 promotes the activation of lung fibroblasts by modulating the alternative splicing of the *PKM* gene. Specifically, SRSF7 enhanced exon 2 skipping on the *PKM* pre-mRNA, leading to the formation of the *PKM△E2* isoform, a finding observed in lung tissue from IPF patients.

PKM encodes pyruvate kinase, a key enzyme in glycolysis, which includes mutually exclusive exons 9 and 10 that give rise to the isoforms PKM1 and PKM2, respectively. These isoforms exhibit distinct functional roles in various diseases[37,38]. Among them, PKM2 (pyruvate kinase M2) catalyzes the final step of glycolysis and is highly expressed in embryonic cells. PKM2 undergoes complex allosteric regulation to execute diverse biological functions[39]. Previous studies have demonstrated that PKM2 promotes pulmonary fibrosis by stabilizing the TGF-β1 receptor I, thereby enhancing TGF-β1 signaling[40]. Additionally, mechanical ventilation has been implicated in inducing pulmonary fibrosis by upregulating PKM2 expression, which accelerates aerobic glycolysis[41]. Nonsense mutations and frame-shifting splicing errors can induce premature termination codons (PTC) in mRNA transcripts, resulting in the production of truncated and dysfunctional proteins[42]. In eukaryotic cells, mRNA containing PTCs is selectively degraded by the surveillance mechanism known as Nonsense-Mediated mRNA Decay (NMD)[43]. Given that PKM undergoes alternative splicing in response to increased SRSF7 expression, which could lead to potential NMD-induced degradation and loss of protein-encoding capacity, we retrieved *PKM* transcript information from the NCBI database. Among the transcripts, we focused on *PKM* (NM_001411081.1) and the *PKM⊿E2* isoform (XM_011521670.2), both of which retain the ability to encode functional proteins. To further elucidate the distinct functional roles of these two splicing isoforms, we generated plasmid vectors expressing HA-tagged PKM and PKMΔE2 proteins. Western blot analysis confirmed successful overexpression of both PKM and PKMΔE2, providing a foundation for subsequent functional studies.

In this study, we found that the kinase activity of PKM⊿E2 was significantly higher than that of PKM. Further Seahorse analysis confirmed that PKMΔE2 promoted glycolysis, thereby accelerating fibrogenesis in fibroblasts. Metabolic dysregulation is known to influence the progression of IPF[44]. Previous studies have reported that lung fibroblasts adopt a distinct glycolytic program, and key enzymes involved in glycolysis are upregulated in fibroblasts and myofibroblasts derived from IPF patients[45]. Additionally, glycolysis is essential for the establishment and maintenance of pro-fibrotic phenotypes[46]. Our work provides novel evidence revealing that SRSF7 directly binds to and regulates the AS of *PKM* in lung fibroblasts, leading to glycolytic dysregulation and contributing to the amelioration of pulmonary fibrosis. Furthermore, we validated, for the first time, the direct binding interaction between SRSF7, PKM, and the spliceosome, which establishes a mechanistic foundation for the activation of fibroblasts and the acceleration of aerobic glycolysis.

Based on our results, we propose that the SRSF7/PKM axis may represent a novel therapeutic target for the prevention or treatment of pulmonary fibrosis. To validate this hypothesis, we generated tissue-specific transgenic mice and investigated whether SRSF7 deficiency could alleviate BLM-induced pulmonary fibrosis in mice. The results demonstrated that reduced expression of SRSF7 significantly abrogated the pro-fibrotic effects of BLM in the mice. To further elucidate the protective role of SRSF7 inhibition in pulmonary fibrosis, we screened for FDA-approved drugs that target SRSF7 activity and confirmed their anti-fibrotic effects in mice. To the best of our knowledge, this study represents the first comprehensive evaluation of the role of SRSF7 in pulmonary fibrosis, as well as its regulation by specific mediators and pharmacologic agents within fibroblasts.

However, there are several limitations to our present study. First, although we demonstrated that upregulation of SRSF7 in fibroblasts induced glycolytic dysregulation, we did not determine whether the accumulation of lactate might affect histone lactylation, despite the well-established evidence that histone lactylation promotes macrophage profibrotic activity. Second, we cannot exclude other mechanisms apart from Lomitapide that may alleviate experimental lung fibrosis. The aberrant alternative splicing events of PI3K−AKT-related genes may also play a role in the pathological mechanism of *Srsf7*-cKO lung, but the aberrantly spliced isoforms of these genes remain poorly understood and require further investigation. Therefore, more comprehensive studies are warranted to determine how alternative splicing contributes to fibrosis-related diseases.

5. Conclusions

This study identified SRSF7, an RNA splicing factor, as a regulator of the alternative splicing of *PKM*, which subsequently leads to dysregulation of glycolysis and activation of fibroblasts. This study not only uncovers a novel role for SRSF7 in the lung but also indicates that targeting the SRSF7−*PKM* axis can provide a new therapeutic strategy for treating pulmonary fibrosis.

Acknowledgments

We appreciate Dr. Zhixin Li very much for providing the tissue samples from patients with and without IPF, and the early contributions to the project. This study was supported by the National Natural Science Foundation of China (U24A20645, 32171127, 82200070), the Scientific Fund Project of Heilongjiang Province (JQ2022H001, China), the Science and technology project of Xiamen Medical College (K2023-08, China) and the CAMS Innovation Fund for Medical Sciences (CIFMS, 2019-I2M-5-078, China).

Author contributions

Tongzhu Jin: Investigation, Methodology, Writing—original draft. Huiying Gao and Yuquan Wang: Conceptualization, Writing—original draft. Zhiwei Ning: Data curation, Visualization. Danyang Bing, Yan Wang, Yi Chen and XiaomuTian: Investigation, Methodology. Qiudi Liu, Zhihui Niu and Ruoxuan Yang: Data curation, Visualization. Jiayu Guo, Shifen Li and Jian Sun: Conceptualization. Tianyu Li and Yuhong Zhou: Project administration, Supervision. Haihai Liang, Yunyan Gu, Wenxin He and Yanjie Lu: Conceptualization, Funding acquisition, Writing — review & editing.

Conflicts of interest

The authors declared no conflict of interest.

Appendix A. Supporting information

Supporting information to this article can be found online at https://doi.org/10.1016/j.apsb.2025.04.017.

References

1. Cui H, Xie N, Banerjee S, Ge J, Jiang D, Dey T, et al. Lung myofibroblasts promote macrophage profibrotic activity through lactate-induced histone lactylation. *Am J Respir Cell Mol Biol* 2021;**64**: 115−25.
2. Raghu G, Collard HR, Egan JJ, Martinez FJ, Behr J, Brown KK, et al. An official ATS/ERS/JRS/ALAT statement: idiopathic pulmonary fibrosis: evidence-based guidelines for diagnosis and management. *Am J Respir Crit Care Med* 2011;**183**:788−824.
3. Richeldi L, Collard HR, Jones MG. Idiopathic pulmonary fibrosis. *Lancet* 2017;**389**:1941−52.
4. Zhao L, Zhu Y, Tao H, Chen X, Yin F, Zhang Y, et al. Ailanthone ameliorates pulmonary fibrosis by suppressing JUN-dependent MEOX1 activation. *Acta Pharm Sin B* 2024;**14**:3543−60.
5. Fortier SM, Walker NM, Penke LR, Baas JD, Shen Q, Speth JM, et al. MAPK phosphatase 1 inhibition of p38alpha within lung myofibroblasts is essential for spontaneous fibrosis resolution. *J Clin Investig* 2024;**134**:e172826.
6. Li Y, Jiang D, Liang J, Meltzer EB, Gray A, Miura R, et al. Severe lung fibrosis requires an invasive fibroblast phenotype regulated by hyaluronan and CD44. *J Exp Med* 2011;**208**:1459−71.
7. White ES, Thannickal VJ, Carskadon SL, Dickie EG, Livant DL, Markwart S, et al. Integrin alpha4beta1 regulates migration across basement membranes by lung fibroblasts: a role for phosphatase and tensin homologue deleted on chromosome 10. *Am J Respir Crit Care Med* 2003;**168**:436−42.
8. Isaac R, Bandyopadhyay G, Rohm TV, Kang S, Wang J, Pokhrel N, et al. TM7SF3 controls TEAD1 splicing to prevent MASH-induced liver fibrosis. *Cell Metab* 2024;**36**:1030−43.e7.
9. Guo P, Jiang J, Chu R, He F, Ge M, Fang R, et al. GRK2 mediated degradation of SAV1 initiates hyperplasia of fibroblast-like synoviocytes in rheumatoid arthritis. *Acta Pharm Sin B* 2024;**14**:1222−40.
10. Zou C, Zan X, Jia Z, Zheng L, Gu Y, Liu F, et al. Crosstalk between alternative splicing and inflammatory bowel disease: basic mechanisms, biotechnological progresses and future perspectives. *Clin Transl Med* 2023;**13**:e1479.
11. Li D, Yu W, Lai M. Towards understandings of serine/arginine-rich splicing factors. *Acta Pharm Sin B* 2023;**13**:3181−207.
12. Ule J, Blencowe BJ. Alternative splicing regulatory networks: functions, mechanisms, and evolution. *Mol Cell* 2019;**76**:329−45.
13. Tong J, Li D, Meng H, Sun D, Lan X, Ni M, et al. Targeting a novel inducible GPX4 alternative isoform to alleviate ferroptosis and treat metabolic-associated fatty liver disease. *Acta Pharm Sin B* 2022;**12**: 3650−66.
14. Matlin AJ, Clark F, Smith CW. Understanding alternative splicing: towards a cellular code. *Nat Rev Mol Cell Biol* 2005;**6**:386−98.
15. Wang Z, Burge CB. Splicing regulation: from a parts list of regulatory elements to an integrated splicing code. *RNA* 2008;**14**:802−13.
16. Baralle FE, Giudice J. Alternative splicing as a regulator of development and tissue identity. *Nat Rev Mol Cell Biol* 2017;**18**:437−51.
17. Beazley-Long N, Hua J, Jehle T, Hulse RP, Dersch R, Lehrling C, et al. VEGF-A165b is an endogenous neuroprotective splice isoform of vascular endothelial growth factor A *in vivo* and *in vitro*. *Am J Pathol* 2013;**183**:918−29.
18. Roberts AL, Mavlyutov TA, Perlmutter TE, Curry SM, Harris SL, Chauhan AK, et al. Fibronectin extra domain A (FN-EDA) elevates intraocular pressure through Toll-like receptor 4 signaling. *Sci Rep* 2020;**10**:9815.
19. Liang D, Lin WJ, Ren M, Qiu J, Yang C, Wang X, et al. m^6A reader YTHDC1 modulates autophagy by targeting SQSTM1 in diabetic skin. *Autophagy* 2022;**18**:1318−37.
20. Jin X. Regulatory network of serine/arginine-rich (SR) proteins: the molecular mechanism and physiological function in plants. *Int J Mol Sci* 2022;**23**:10147.
21. Gonzalez-Rodriguez P, Klionsky DJ, Joseph B. Autophagy regulation by RNA alternative splicing and implications in human diseases. *Nat Commun* 2022;**13**:2735.
22. Latorre E, Harries LW. Splicing regulatory factors, ageing and age-related disease. *Ageing Res Rev* 2017;**36**:165−70.
23. Chen S, Yang C, Wang ZW, Hu JF, Pan JJ, Liao CY, et al. CLK1/SRSF5 pathway induces aberrant exon skipping of METTL14 and Cyclin L2 and promotes growth and metastasis of pancreatic cancer. *J Hematol Oncol* 2021;**14**:60.
24. Guo R, You X, Meng K, Sha R, Wang Z, Yuan N, et al. Single-cell rna sequencing reveals heterogeneity of Myf5-derived cells and altered myogenic fate in the absence of SRSF2. *Adv Sci (Weinh)* 2022;**9**: e2105775.
25. Hong J, Min S, Yoon G, Lim SB. SRSF7 downregulation induces cellular senescence through generation of MDM2 variants. *Aging (Albany NY)* 2023;**15**:14591−606.
26. Jeong S. SR proteins: binders, regulators, and connectors of RNA. *Mol Cell* 2017;**40**:1−9.
27. Grosse S, Lu YY, Coban I, Neumann B, Krebber H. Nuclear SR-protein mediated mRNA quality control is continued in cytoplasmic nonsense-mediated decay. *RNA Biol* 2021;**18**:1390−407.
28. Sun J, Jin T, Su W, Guo Y, Niu Z, Guo J, et al. The long non-coding RNA PFI protects against pulmonary fibrosis by interacting with splicing regulator SRSF1. *Cell Death Differ* 2021;**28**:2916−30.
29. Muller-McNicoll M, Botti V, de Jesus Domingues AM, Brandl H, Schwich OD, Steiner MC, et al. SR proteins are NXF1 adaptors that link alternative RNA processing to mRNA export. *Genes Dev* 2016; **30**:553−66.
30. Shen W, Yuan L, Cheng F, Wu Z, Li X. SRSF7 is a promising prognostic biomarker in hepatocellular carcinoma and is associated with immune infiltration. *Genes Genom* 2024;**46**:49−64.
31. Fu Y, Wang Y. SRSF7 knockdown promotes apoptosis of colon and lung cancer cells. *Oncol Lett* 2018;**15**:5545−52.
32. Schwich OD, Blumel N, Keller M, Wegener M, Setty ST, Brunstein ME, et al. SRSF3 and SRSF7 modulate 3′UTR length through suppression or activation of proximal polyadenylation sites and regulation of CFIm levels. *Genome Biol* 2021;**22**:82.
33. Bustos F, Segarra-Fas A, Nardocci G, Cassidy A, Antico O, Davidson L, et al. Functional diversification of SRSF protein kinase to control ubiquitin-dependent neurodevelopmental signaling. *Dev Cell* 2020;**55**:629−47.e7.
34. Blencowe BJ. Alternative splicing: new insights from global analyses. *Cell* 2006;**126**:37−47.
35. Kadota Y, Jam FA, Yukiue H, Terakado I, Morimune T, Tano A, et al. Srsf7 establishes the juvenile transcriptome through age-dependent alternative splicing in mice. *iScience* 2020;**23**:101242.
36. Fu Y, Huang B, Shi Z, Han J, Wang Y, Huangfu J, et al. *SRSF1* and *SRSF9* RNA binding proteins promote Wnt signalling-mediated tumorigenesis by enhancing beta-catenin biosynthesis. *EMBO Mol Med* 2013;**5**:737−50.
37. Li Y, Zhang S, Li Y, Liu J, Li Q, Zang W, et al. The regulatory network of hnRNPs underlying regulating PKM alternative splicing in tumor progression. *Biomolecules* 2024;**14**:566.
38. Demeter JB, Elshaarrawi A, Dowker-Key PD, Bettaieb A. The emerging role of PKM in keratinocyte homeostasis and pathophysiology. *FEBS J* 2023;**290**:2311−9.
39. Wu X, Liu L, Zheng Q, Hao H, Ye H, Li P, et al. Protocatechuic aldehyde protects cardiomycoytes against ischemic injury *via* regulation of nuclear pyruvate kinase M2. *Acta Pharm Sin B* 2021;**11**: 3553−66.
40. Gao S, Li X, Jiang Q, Liang Q, Zhang F, Li S, et al. PKM2 promotes pulmonary fibrosis by stabilizing TGF-beta1 receptor I and enhancing TGF-beta1 signaling. *Sci Adv* 2022;**8**:eabo0987.
41. Mei S, Xu Q, Hu Y, Tang R, Feng J, Zhou Y, et al. Integrin beta3-PKM2 pathway-mediated aerobic glycolysis contributes to

mechanical ventilation-induced pulmonary fibrosis. *Theranostics* 2022;**12**:6057−68.
42. Pervouchine D, Popov Y, Berry A, Borsari B, Frankish A, Guigo R. Integrative transcriptomic analysis suggests new autoregulatory splicing events coupled with nonsense-mediated mRNA decay. *Nucleic Acids Res* 2019;**47**:5293−306.
43. Isken O, Maquat LE. The multiple lives of NMD factors: balancing roles in gene and genome regulation. *Nat Rev Genet* 2008;**9**: 699−712.
44. Roque W, Romero F. Cellular metabolomics of pulmonary fibrosis, from amino acids to lipids. *Am J Physiol Cell Physiol* 2021;**320**: C689−95.
45. Parimon T, Hohmann MS, Yao C. Cellular senescence: pathogenic mechanisms in lung fibrosis. *Int J Mol Sci* 2021;**22**:6214.
46. Goodwin J, Choi H, Hsieh MH, Neugent ML, Ahn JM, Hayenga HN, et al. Targeting hypoxia-inducible factor-1alpha/pyruvate dehydrogenase kinase 1 axis by dichloroacetate suppresses bleomycin-induced pulmonary fibrosis. *Am J Respir Cell Mol Biol* 2018;**58**:216−31.